Title
THE SCATTERING OF 22-MEV POSITIVE PIONS ON PROTONS

Authors
Whetstone, Stanley L.
Stork, Donald H.

Publication Date
1955-11-01

UNIVERSITY OF CALIFORNIA

Radiation Laboratory

BERKELEY, CALIFORNIA

DISCLAIMER

UCRL-3087 Rev

UNIVERSITY OF CALIFORNIA
Radiation Laboratory
Berkeley, California

Contract No. W-7405-eng-48

THE SCATTERING OF 22-Mev POSITIVE PIONS ON PROTONS

Stanley L. Whetstone, Jr. and Donald H. Stork

November 1955

Printed for the U. S. Atomic Energy Commission

THE SCATTERING OF 22-Mev POSITIVE PIONS ON PROTONS

Stanley L. Whetstone, Jr.*† and Donald H. Stork

Radiation Laboratory
University of California
Berkeley, California

November 1955

ABSTRACT

The differential cross section for the reaction $\pi^+ + p \rightarrow \pi^+ + p$ was measured in the angular interval 45° to 135° in the center-of-mass system at a pion energy of 21.5 ± 3.5 Mev in the laboratory system.

The pion beam was formed by a magnetic-focusing selection of pions produced from polyethylene at an angle of 0° in the reaction $p + p \rightarrow \pi^+ + d$. The production target was placed in the strong-focused 340 Mev proton beam electrostatically deflected from the Berkeley synchrocyclotron. The pion beam entered liquid hydrogen contained in a styrofoam scattering target at 25.0 Mev, with an energy spread of ± 0.6 Mev, and left at 18.0 Mev.

Scattered pions were detected in an emulsion stack placed 1 inch from the beam edge and 7/8 inch from the liquid hydrogen. The data, consisting of 41 acceptable events, were analyzed by a maximum-likelihood method to obtain the following best values for the pion-proton scattering phase shifts at a relative momentum, $\eta = 0.49$:

$$a_3 = -0.048 \pm 0.007 , \quad a_{33} = +0.013 \pm 0.013 , \quad a_{31} = 0.000 \pm 0.016 .$$

I. INTRODUCTION

The study of pion-proton scattering has already provided considerable information concerning the interaction in the lowest two angular momentum states, usually expressed in terms of the S- and P-wave phase shifts. The behavior of the $P_{3/2}$ phase shift for the state of total isotopic spin $T = 3/2$, which largely determines the scattering cross section at pion energies between about 30 and 300 Mev by its "resonant" behavior in the neighborhood of 180

---

*Now at Los Alamos Scientific Laboratory.

†Thesis.

Mev, has been rather well determined by experiments in this energy region, and quite well explained by a phenomenological meson theory.[1-3]

The behavior of the S-wave phase shifts, which have an appreciable effect on the cross sections only at low energies, is less well-known experimentally, and has been a subject of debate among theorists. At the time this experiment was begun, the available experimental data[1] (from the Panofsky effect at zero energy and the pion-proton scattering at energies higher than about 33 Mev) indicated quite strongly that the T = 3/2, S-wave phase shift, although negative at the higher energies, changed sign at about 20 Mev and approached zero energy with a positive slope. Several experiments to determine the S-wave phase shift for positive pion-proton scattering at about 20 Mev have been attempted. The preliminary results of the scattering-in-emulsion experiment of Orear[4] indicate that the S-wave phase shift is sufficiently negative at 20 Mev to preclude any cross over in this energy region. Meanwhile, the zero-energy data have been improved, with valuable information obtained from the study of mesic atoms, so that the original requirement that the S-wave phase shift approach zero energy with a positive slope was invalidated.[2]

The specification of the over-all sign of the phase shifts was also, until recently, uncertain.[5] At the time, the only method used to determine this over-all sign was to note the effect on the angular distribution of the interference between the nuclear scattering amplitudes and the amplitudes for the Coulomb scattering, the signs of the latter being known for interacting particles of known charge. At low energies the effect of the coulomb interaction extends to scattering angles large enough to be experimentally accessible. Measurements of the angular distribution of the scattering in the region from 40 to 65 Mev,[6] however, could not establish the behavior of the interference because of a chance near canceling of the nuclear part of the scattering amplitude in the angular region where the interference predominates. Experiments near 120 Mev[7] (where the scattering cross sections are large), performed using the scattering-in-emulsion method--in which the cross sections could be determined down to fairly small angles--permitted a rather definite determination of the interference, with which the present experiment is in agreement. More recently, it has been shown that application of causality requirements to the general scattering theory requires a positive sign for the T = 3/2, $P_{3/2}$ phase shift,[8] in view of the resonance behavior of this phase shift.

The experimental study of pion-proton scattering in the lower-energy region is rendered increasingly more difficult by the smaller scattering cross sections involved, the lower flux of the available pion beams, and the shorter range and greater multiple Coulomb scattering in the targets and detectors. One successful solution to these problems is the emulsion technique, where scatters from the hydrogen in the emulsion gelatin are recognized from the kinematics of the observed events. Studies are also being made using high-pressure hydrogen-filled diffusion cloud chambers.[9]

The method we have adopted requires that the scattered pions escape from a liquid hydrogen target and reach an emulsion stack with an energy great enough to permit an accurate measurement of the scattering direction. Our method recommends itself chiefly because of the relatively rapid collection of scattering events it provides. This is a particularly important consideration, since the limiting factor in the study of the low-energy pion-proton scattering by the methods available at present is the slow rate of data collection.

II. THE EXPERIMENTAL APPARATUS AND PROCEDURE

The general arrangement of the apparatus in the experimental area is shown in Fig. 1.

Formation of the Pion Beam

A low-energy pion beam of sufficient flux and adequate energy resolution was formed by the following means:

Advantage was taken of the very large cross section for the production of positive pions at forward angles in the reaction $p + p \rightarrow \pi^+ + d$.[10] The incident protons were obtained from the 340-Mev proton beam electrostatically deflected from the 184-inch synchrocyclotron. Target protons were provided by the hydrogen in polyethylene, $(CH_2)_x$. The target thickness was chosen to provide the energy degradation required to give pions produced in the above reaction at 0° to the beam at the center of the target the desired energy on emergence from the polyethylene. Because of a degradation of the proton beam that is very nearly compensating for hydrogenous materials,[11] pions produced at 0° elsewhere in the target will have very nearly the same emergence energy. An analyzing magnet was used to deflect the pions produced in this fashion away from the higher-momentum beam protons and into a collimator that lead to the liquid hydrogen scattering target.

Advantage was taken also of the double-focusing properties of the magnetic field provided by the analyzing magnet's wedge-shaped pole piece. Several geometries for double-focus conditions were first determined for the simple case of an infinitely narrow fringe field, following Camac.[12] The optimum case was chosen and checked by the following procedure: an analogue computing machine, known as the "the mechanical particle,"[13] was used to trace out, on a full-scale contour plot of the magnetic field, central trajectories. The vertical or horizontal focus points were found by considering trajectories deviating slightly from the central trajectory and numerically integrating the first-order equations of motion. A significant change in the original calculated focus conditions was found necessary. The central trajectories were finally checked in the magnet itself by use of a flexible current-carrying wire held in tension in the field.

To ensure a sufficient flux of pions through the scattering target, it was necessary to concentrate vertically the proton beam at the production target. Concentration of the proton beam horizontally, as well, improved the energy resolution. Three pairs of quadrupole strong-focusing magnets,[14] one "lens" at the exit of the proton beam steering magnet and the other two in the target area, were used to focus the 2-inch diameter proton beam into an area roughly 3/8 inch wide and 3/4 inch high at the production target.

To avoid scattering by air and thus increase the efficiency of the focusing, the proton beam was brought up to the production target, through the quadrupole magnets, in a pipe providing an extension of the vacuum system of the cyclotron. Replacing the air in the path of the pion beam with helium gas reduced the calculated rms lateral deviation at the scattering target due to multiple Coulomb scattering by a factor of five, to approximately 5/8 inch. The helium was contained in a large 0.004-inch-thick polyethylene bag, which bulged out from between the magnet pole pieces up against the production target, and which was sealed around the collimator opening. The other end of the pion beam collimator pipe was sealed against the styrofoam jacket of the scattering target to close the system. A small bag of the same polyethylene material was connected to the system outside the shielding, where it was always accessible for visual and tactual monitoring of the helium pressure.

The Counter Telescope

The counter telescope consisted of a 1-inch-thick polystyrene-terphenyl plastic scintillator, 1.5 inches in diameter, placed 1.25 inches behind an anthracene crystal 3/4 by 3/4 by 1/8 inch both viewed by Dumont 6292 photomultiplier tubes.

Situated in the pion beam behind the scattering target, the counter telescope provided a continuous monitor of the pion beam flux. The counters were thus indispensable during the initial forming of the beam. The pion to proton flux ratio was found to remain constant, within the limitations of the instruments, throughout the experiment. By placing various thicknesses of copper absorber between the two crystals, integral range curves were obtained, from which the pion beam energy was determined.

It should be pointed out that the cross sections measured in this experiment do not depend on the counting system. Measurements of the pion beam energy were obtained independently from pion ranges in several emulsion stacks.

The Liquid Hydrogen Scattering Target

Details of the target structure are shown in Figs. 2 and 3. The recently developed material, expanded polystyrene, $(CH)_x$ (better known by the trade name, styrofoam), provided an efficient insulating jacket which interfered little with the scattering process and permitted the close approach of the emulsion detector to the target protons.

The actual target volume was defined by the pion beam cross-sectional area and by the length of the hydrogen container. This length represents a compromise between a large number of scattering centers and a small energy loss in the target. The necessary use of a beam of large cross-sectional area, and the desire not to include scattering events from the directions of the carbon-rich ends of the target, argued for the length chosen: 3.5 inches.

Several attempts to use the styrofoam jacket as the actual container of the liquid hydrogen proved unsuccessful. After some trial, it was found that polyethylene sheet could be fabricated into a leakproof container for liquid hydrogen. The welding of satisfactory joints was accomplished with commercially available hot-air guns. Shrinkage of the expected amount was observed when the container was filled with liquid nitrogen, and the warping was not serious. The container, of 0.040-inch polyethylene, was cut away in the area of the beam entrance and exit and along the entire side facing the emulsion stack detector.

This area was covered with 0.004-inch polyethylene foil, stretched tight and welded to the heavier container.

The styrofoam jacket was everywhere at least 2 inches thick, except for the 5/8-inch thin wall facing the emulsion stack, and a small 1-inch thick beam entrance window. The jacket was made in two pieces which fit together by a tongue-and-groove joint, sealed with silicone grease, and pulled together by rods reaching from the plywood top and bottom plates. The target was designed to force the evaporating hydrogen vapor to flow down and around the sides of the polyethylene container before passing through the jacket to the exhaust hose. Despite this design, the measured evaporation rate was about 7 liters/hour, requiring a refill every 20 to 25 minutes.

The level of the liquid was indicated by a long straw glued to a styrofoam float. For insurance and convenience, the target was also fitted with a sensing element which consisted of a cylindrical nickel capacitor connected to the tuning circuit of a simple radio transmitter. The relation between the liquid height in the capacitor and the frequency of the radio signal was easily found by calibration against the float.

The emulsion stack detector was held in a drawerlike lucite holder, which slid into a hole in the styrofoam jacket at the side of the target and permitted an accurate determination of the detector position and orientation. The holder was designed so that warmed helium gas could be passed across the face of the emulsion stack, in an attempt to keep the emulsion temperature well above the temperature of the liquid hydrogen. At liquid hydrogen temperature the sensitivity of the emulsion is reported to be zero.[15] During each of the two days the stack was exposed, the temperature at the stack face was monitored with an iron-constantan thermocouple. This temperature was typically from -10 to -20°C, except for brief periods the first day when overfilling of the liquid hydrogen container dropped the reading to the neighborhood of -80°C. Even at these lowest temperatures, the emulsion sensitivity is reported[16] to be decreased by only a factor of two, so that all tracks of scattered pions should still have been visible.

The Emulsion Stack Detector

To be able to observe with ease and assurance the tracks of the scattered pions entering the emulsion detector with energies up to 25 Mev (with ionization down to about twice minimum), it was considered advisable to use the highly

sensitive Ilford G. 5 emulsion. This choice was also insurance against any decrease in emulsion sensitivity at the temperatures to which it would be subjected at a distance of one inch from the liquid hydrogen in the target.

The emulsion stack detector consisted of a stack of 60 Ilford G. 5 pellicles 6 by 1.7 inches by 600 microns, bolted tightly together between two sheets of 0.25-inch black bakelite by stainless steel screws.[17] The screws passed through holes, punched in the individual emulsions with a simple jig, in positions beyond the range of the scattered pions. Once the screws were tightened the stack could be exposed to daylight. All edges of the stack were then milled smooth and to the desired dimensions. X-ray marks were placed in the stack to facilitate the later realignment of the individual processed layers. The milled front surface permitted a more accurate measure of the ranges of the scattered pions.

After the exposure, the stack was unbolted and the layers were stripped apart and mounted on glass slides. The chemical processing processing procedure followed closely that developed by the Bristol Group for thick G. 5 emulsion.[18]

To simplify the relative alignment of the emulsion layers, brass tabs were glued across the two back corners of the glass mounts. With the stage stops of the scanning microscope for reference the tabs were then systematically sanded down until the X-ray lines came into approximate coincidence in the field of view. Alignment to ± 50 microns was very easily attained; follow-through track shift near the plate edge caused by misalignment was smaller than that resulting from emulsion distortion.

Scanning Procedure

The range of a 25-Mev pion in G. 5 emulsion is approximately 11.5 mm. The scattered pions were therefore confined to the volume within at most 12.5 mm from the front edge of each of the 60 plates. One method of locating all the scattered pion tracks would be simply to scan "by area" this entire volume plate by plate, looking for the positive pion endings. Another method, suggested by the relatively low number of background tracks and the possibility of following through tracks from one plate to the next, was to scan just one swath along the front edge of each plate, following every track that showed a likelihood of being a pion, until the likelihood was decisively reduced in some way--excessive range, non follow-through (prestacking background amounted to some 20%), proton endings, star events, etc. --or until the likelihood was rendered a certainty by the recognition of the characteristic pion ending.

The second method was used; although, to make it certain that every pion track would be seen, it was found necessary to take the swath a distance of 3 mm from the emulsion edge. (The quality of our processed emulsion deteriorated rapidly as the edge was approached.) The swaths at 3.0 mm thus determined the solid angle of the detector, the endings in the region nearer the plate edge were picked up by area scanning.

All of the scanning was done with 10x wide-field oculars and 22x oil-immersion objectives. The field diameter of nearly 1.0 mm expedited the area scanning and provided a track selection swath sufficiently broad to allow for any misalignment due to emulsion distortion. The use of an oil-immersion objective for the follow through was found to be advisable to obtain the visibility required for picking up all the tracks. With practice it became possible to follow through under oil, with the Leitz normal-working-distance 22x objective, very nearly as rapidly as with an air objective.

Rough checks of the follow-through scanning efficiency were made by rescanning several centimeters of swath and comparing the track-following records. Since the area scanning overlapped the follow-through swath by several millimeters, it was possible to check the area scanning efficiency against the eighty-odd pion endings in the area-scanned region found mostly at random in the course of the follow-through scanning.

A pion track recognition efficiency of 95 ± 5% is believed. The loss uncertainty here adds little to the over all statistical uncertainty of the experimental results.

III. THE EXPERIMENTAL DATA

The Pion Beam

1. Energy Measurements. The energy of the pion beam was measured periodically during the exposure, with and without liquid hydrogen in the beam, by two independent methods: integral range measurements in copper with the counters, and projected range measurements in emulsion stacks.

a. Integral range measurements. A pair of integral range curves are shown in Fig. 4. The points, as plotted, include an addition of 0.072 g/cm^2, the equivalent copper range required in the back counter for a pulse greater than the discrimination level. The ranges at half height (a good measure of the mean ranges in this case, since the incident beam was nearly monoenergetic)

are 3.80 ± 0.22 g/cm^2 and 1.55 ± 0.22 g/cm^2 for target out and for filled target in, respectively. The uncertainties represent a rough estimate of the range spread at half maximum of the differential range curves. The mean ranges at the front of the copper absorbers, corrected for scattering, are 3.95 and 1.60 g/cm^2, corresponding to 23.9 and 14.2 Mev according to the range-energy curves of Aron.[19] The energy of the pion beam is found to be 25.5 ± 0.5 Mev into the liquid hydrogen and 18.4 ± 0.3 Mev out. This corresponds to passage through a thickness of 8.61 cm of liquid hydrogen, a thickness just 3.3% less than the designed length of the target. This would indicate that neither the shrinkage nor the bubbling was serious.

The mean ranges determined from three other integral range curves agree to within about 1.5% with the corresponding mean ranges obtained above, although these curves were not quite as complete as the two analyzed above. This indicates that the energy of the pion beam varied less than 1% over the two days of the scattering exposure.

b. Projected range measurements. Samples of the pion beam were taken with emulsion stacks during the two days of the scattering exposure. Typical projected range distributions in emulsion are given in Fig. 5. The analysis of these distributions to determine the mean energy and rms spread of the pion beam into and out of the liquid hydrogen may be summarized as follows: The measured projected ranges (mean and rms deviation) are 11.15 ± 0.75 and 5.29 ± 0.75 mm, for target out and hydrogen in, respectively. The mean ranges corresponding to the above, obtained by correcting for the scatter-shortening, are 11.80 and 5.61 mm. These mean ranges correspond to mean energies into the emulsion of 25.4 and 16.55 Mev,[20] or to calculated mean energies into and out of the liquid hydrogen, of 24.9 and 17.9 Mev, respectively. An effective target length 4.8% shorter than designed is indicated. The calculated rms energy spreads into and out of the liquid hydrogen, corrected for the small (3%) energy straggling in the emulsion, are ± 0.8 and ± 1.2 Mev, respectively. The true energy spreads of the beam are smaller than these, because of the contribution of the scatter-straggling to the measured spread.

An analysis of a projected range distribution, obtained during the other day of the exposure, gives 17.6 Mev for the mean energy out of the liquid hydrogen--in good agreement with the value 17.9 Mev found above.

It is believed that more weight should be given to the emulsion measurements of the beam energies than to the measurements made with the counters and copper absorbers. We thus believe the pion beam energy to have been

$25.0 \,^{+0.5}_{-0.2}$ Mev, with rms spread ± 0.6 Mev, into the liquid hydrogen, and 18.0 Mev out. This corresponds to a mean energy of 21.5 Mev.

2. The Spatial Beam Distribution. Pion beam intensity distributions, measured in emulsion stacks across the approximate beam center in both the horizontal and vertical planes, are presented in Fig. 6. The vertical distribution was obtained at the exit of the collimator the first day of the scattering exposure. The symmetric trapezoid (dashed lines) represents the distribution expected at the collimator exit, assuming a uniform diffuse source of pions across the collimator entrance aperture, and using the average of the central points for the value of the "full beam" intensity.

The horizontal distribution, although not so likely to be affected by the focusing, was also checked.

3. The Total Number of Pions Through the Target. With the ratio of pions through the target to protons through the ionization chamber constant, the total number of pions was determined from the total integrated proton beam current, the average number of pions found per unit area per unit integrated proton beam current in the full-intensity regions of the beam-sampling monitor stacks, and the total equivalent full-intensity area of the beam in the scattering target. Before averaging, pion fluxes measured at different distances from the pion source (taken to be the collimator entrance aperture) were normalized to the center of the scattering target (an inverse-square dependence was assumed).

Four samples of the pion beam, taken over the two days of the exposure, were analyzed and found mutually consistent with respect to the number of pions per unit area per unit integrated proton beam current. The total "two-day" exposure yielded 1.12×10^3 pions per square mm, a total number of pions through the target, $N = 1.73 \pm 0.08 \times 10^6$. (The pion flux averaged about 9 per square inch per second.)

B. The Scattered Pions

Tracks of scattered pions entering the face of an emulsion stack detector possess information essential for the reconstruction of the kinematics of the individual scattering events.

1. The Measurements. A measurement of the projected and dip angles α, δ specifies the direction of the scattered pion. Since the direction of the incident pion beam is known, this permits a direct calculation of the polar and azimuthal

scattering angles θ, ϕ. A measurement of the point of entrance into the stack then specifies the actual line of scatter. Since the position of the stack with respect to the liquid hydrogen target is known, this permits the rejection of scatters not passing through the target, as well as those coming from the direction of the front and back ends of the target. A measurement of the residual range of the pion at the stack face R_o specifies the entrance energy E_o there. From the above information it is possible to reconstruct the scattering event by making the assumption that the scatter occurred at either the near or the far edge of the effective target. At the near edge, defined by the thin polyethylene window, the scatter could possibly have been from a carbon atom.

For each of the three assumptions--i.e., elastic carbon or hydrogen event at the near side or hydrogen event at the far side of the target--it is possible to calculate the expected energy of the pion indicent on the liquid hydrogen. The three estimated incident energies may be compared with the known pion beam energy into the liquid hydrogen. The two estimations for hydrogen scattering represent the lower and upper bounds for the estimated energy, assuming the event to have taken place in the target volume. For true hydrogen events, these bounds should bracket the beam energy, to within the limits of experimental error and the beam energy spread. For true carbon events, the estimated energy should coincide, to within similar limits, with the beam energy. The result of this analysis of all of the otherwise acceptable scattering events, found in the center of mass angular interval $35^\circ < \chi < 135^\circ$, is presented in Fig. 7. Two certain and three possible carbon events are indicated.

All measurements were made using 6x oculars and a 53x oil objective. The most important measurement, that of the projected scattering angle α, was made with an eyepiece goniometer. The dip angle δ was determined by measuring the coordinates of two points on the track, one as near the stack-face edge as the distortion and blackening would permit, the other 400 to 800 microns removed. The vertical coordinates, measured with the calibrated fine-focus adjustment, were all corrected for the emulsion shrinkage by determining the fractional depth in the emulsion and assuming the original thickness to have been 595 microns. (This thickness is equal to the measured net thickness of the emulsion in the clamped stack divided by the total number of pellicles. This value of the thickness, combined with accurate measurements of the length and width of the milled stack and of the net weight of the emulsion, yielded the value 3.80 g/cm^3, in very good agreement with the value 3.81 g/cm^3, commonly obtained.[21]

The emulsion-to-glass bond is strong,[22] the original position of the much distorted edge is preserved there. The point of entry and the length of track through the edge region, could therefore be calculated.

2. Correction for Emulsion Distortion. The distortion of the emulsion near the plate edges was investigated by measurements made on very steep, light tracks that could be followed through many successive layers. Effects of plate misalignment were removed to good approximation by measuring the emulsion edges at the glass. The distortion, as was expected, affected appreciably only the coordinate y, perpendicular to the edge. The y-coordinate distortion shift between the bottom (fixed) surface of one emulsion and the top (displaced) surface of the next was measured along the same steep track through many plates. The results are plotted in Fig. 8. The magnitude of the shift is seen to be quite systematic, decreasing linearly from a value near 160 microns at a distance of 1.0 mm from the edge to 0 at about 11.5 mm. For a first order correction, the shift of the y-coordinate of a track grain may be considered equal to the total shift appropriate for its distance from the emulsion edge, times its height in the emulsion, divided by the total emulsion thickness. This correction to all y-coordinates was made in all measurements.

3. Uncertainties in the Determination of the Scattering Angles. The factors introducing uncertainties in the measured values of the individual scattering angles, θ, and the magnitudes of their respective effects may be summarized as follows: (a) beam divergence, $|\Delta\theta| \leq 2.5^{\circ}$; (b) stack line-up with respect to beam, $|\Delta\theta| < 1^{\circ}$; (c) instrumental limitations (goniometer and microscope coordinate readings), $|\Delta\alpha|$, $|\Delta\delta| < 1^{\circ}$ ($\cos\theta = \cos\alpha \cos\delta$); (d) emulsion distortion, $|\Delta\alpha| = 1 - 2^{\circ}$, $|\Delta\delta| \lesssim 1 - 2^{\circ}$, with use of distortion correction curve; (e) multiple scattering in the liquid hydrogen target and in the entrance edge region of the emulsion. The multiple scattering along the unobservable portion of the trajectories in the emulsion contributes an rms projected angular spread of from 6° at forward and central scattering angles to 8.5° at the extreme backward angles accepted. The contribution to the angular spread due to the multiple scattering in the target aggregate (both before and after scattering) was, for the worst case (E_0 = 10 Mev), about 4°.

The over all uncertainty in the determination of the individual center-of-mass scattering angles, χ, in the range considered, was thus of the order of 7° to 10°.

4. Summary of the Analysis of the Pion Endings. A total of 329 positive-pion endings were located, acceptable in the 12-plate solid angle. Six of these tracks too short to measure, and 211 at the extreme forward angles, $\theta < 30^{\circ}$, were rejected forthwith. Measurements of the remaining tracks found 20 rejected by a minimum range criterion ($E_o < 10$ Mev), 26 not from the direction of the target volume, and 18 from the direction of the front and back ends of the target.

The remaining 48 events found in the center-of-mass angular interval $35^{\circ} \leq \chi \leq 135^{\circ}$ are plotted in Fig. 7. The rejection of the two certain carbon events (labeled C in the figure) results in 41 probable hydrogen events in the interval $45^{\circ} \leq \chi \leq 135^{\circ}$, and 28 in $60^{\circ} \leq \chi \leq 120^{\circ}$. The exclusion of the three possible elastic carbon events (labeled C? in the figure) leaves 38 certain hydrogen events in $45^{\circ} \leq \chi \leq 135^{\circ}$, and 27 in $60^{\circ} \leq \chi \leq 120^{\circ}$.

IV. CALCULATION OF THE DIFFERENTIAL CROSS SECTION

For the purpose of simplifying the calculation of the scattering cross section, the actual pion beam flux distribution through the liquid hydrogen was replaced to sufficiently good approximation by a distribution uniform throughout a suitably chosen rectangular area, A. The expression for the expected number of scatters (in $d\theta$ at θ, from all volume elements of the target) that would enter an infinitely long emulsion layer becomes:

$$\frac{dC(\theta)}{d\theta}\, d\theta = Nn \frac{d\sigma(\theta)}{d\Omega} \sin\theta\, d\theta\, \overline{\Delta\phi}\,,$$

where $\frac{d\sigma(\theta)}{d\Omega}$ is the differential scattering cross section per unit solid angle, θ and ϕ are the laboratory polar and azimuthal scattering angles, N is the total number of pions passed through the scattering volume, and n is the total number of target protons per cm^2 in the target length, L. $\overline{\Delta\phi}$ is the interval of the angle ϕ subtended by the emulsion layer at a point in the target, averaged over the entire target volume.

$$\overline{\Delta\phi} = \frac{1}{AL} \int_{\phi_1}^{\phi_2} \int_{V'} d\phi\, dV\,,$$

where V' represents the boundaries of the idealized target of length L and area normal to the beam, A.

Three considerations complicate the evaluation of the quantity $\overline{\Delta\phi}$ for the actual situation: (a) the finite length of the emulsion layer, (b) the requirement that no scatters come from the direction of a target end, (c) the requirement that only pions entering the stack with energies greater than a specified amount be counted. (The minimum energy limit of 10 Mev at the stack entrance point requires that pions scattering at large angles from the back portions of the target must be excluded.)

The main effect of these conditions is to modify the boundary of the volume integration, V', so that $\overline{\Delta\phi}$ becomes a function of θ. If $\overline{\Delta\phi_o}$ is the mean azimuthal angular interval subtended by a single emulsion layer, the quantity $F(\theta) = \overline{\Delta\phi}/\overline{\Delta\phi_o}$ is a weight factor for the measured angular distribution of the scattering. $F(\theta)$ was determined by means of a semi-analytic calculation. The results, after transformation to the center of mass, are shown in Fig. 9. The weight factor is seen to be close to unity near 90°, corresponding to the nearly total utilization of the target. At the extreme backward angle studied, $\chi = 135^\circ$, $F(\chi)$ introduces a correction factor as large as three. The difference between the solid and broken curves of Fig. 9 represents the correction required to take into account the scattered pions unable to reach the emulsion with energies greater than 10 Mev.

V. THE PHASE-SHIFT ANALYSIS

Theoretical calculations of scattering cross sections are usually compared with the experimental data via the set of parameters--the phase shifts--that characterize the scattering in the partial-wave treatment of the quantum-mechanical scattering system.

The present data has been analyzed under the assumption that only the lowest two orbital angular momentum states (S- and P-waves) contribute significantly to the scattering cross section, and, therefore, that only the S- and P-wave scattering phase shifts are of appreciable magnitude.[23] This assumption should be a very good one in view of the low energy of our incident pions and the failure to find appreciable D-wave phase shifts in the experiments at energies up to 217 Mev.

At energies as low at 22 Mev the Coulomb scattering and the effects of its interference with the nuclear scattering amplitudes are of importance to scattering angles as large as 90°. Several recent treatments of this problem

are available, all of which take advantage of the probable very strong short-range nature of the nuclear force to effect a mathematical separation from the long-range Coulomb force. A convenient relativistic generalization of the Van Hove[24] and Ashkin[25] formulation has been given by Solmitz.[26]

The three scattering phase-shifts, a_3, a_{31}, a_{33}, corresponding to the three angular momentum states $S_{1/2}$, $P_{1/2}$, and $P_{3/2}$, were determined from the experimental data by means of a maximum-likelihood method.[27] This method of adjusting the parameters of a theoretical curve to "best fit" ungrouped data not only permits the maximum utilization of the available information but also is conveniently applied to relatively small amounts of data. The application of this method to these data to obtain the "best values" of the phase shifts may be summarized briefly:

The likelihood function, $L(\chi_1, \chi_2, \ldots, \chi_m; a_3, a_{31}, a_{33})$, expressing the relative "joint probability" of obtaining the set of scattering events at χ_1, $\chi_2, \ldots, \chi_m$, and no events elsewhere, is maximized by varying the individual phase shifts.

The likelihood function is

$$L(\chi \ldots, a \ldots) = \prod_{j=1}^{m} \frac{d\sigma^*}{d\Omega}(\chi_j, a \ldots)\, e^{-M\sigma^*_T(a\ldots)},$$

where

$$M = nNq\,\overline{\Delta\phi_o} = 1.019 \times 10^{29}\ \text{cm}^2,$$

(where q is the number of emulsions scanned), and

$$\frac{d\sigma^*}{d\Omega}(\chi, a \ldots) = F(\chi) \sin\chi\, \frac{d\sigma(\chi, a\ldots)}{d\Omega}\ ;\ \sigma^*_T = \int \frac{d\sigma^*}{d\Omega}\, d\chi\ .$$

The differential scattering cross section is

$$\frac{d\sigma}{d\Omega}(\chi, a \ldots) = \frac{1}{4k^2} \sum_{i=1} A_i^2$$

where

$$\frac{1}{4k^2} = 2.065 \times 10^{-26}\ \text{cm}^2\ ,\ \text{for}\ \eta = \frac{p_{c.m.}}{m_\pi c} = 0.49\ .$$

The scattering amplitudes, in the small-angle approximation, ($\sin a = a$, $\cos a = 1 - \frac{1}{2} a^2$) are: for no spin flip (nf):

$$A_1 = 2a_3 + (4a_{33} + 2a_{31}) \cos \chi + 2\, kf^{(nf)}(\chi)$$

$$A_2 = -2a_3^2 - (4a_{33} + 2a_{31})^2 \cos \chi$$

for spin flip (f);

$$A_3 = (2a_{33} - 2a_{31}) \sin \chi + 2\, kf^{(f)}(\chi)$$

$$A_4 = (-2a_{33}^2 + 2a_{31}^2) \sin \chi$$

The relativistic Coulomb amplitudes[26] are: for no spin flip:

$$f^{(nf)} = \frac{-e^2}{2p(v_\pi + v_p)\sin^2(\chi/2)} \left[1 + \frac{v_\pi v_p}{2c^2}(1 + \cos\chi) + \text{smaller terms}\right]$$

for spin flip:

$$f^{(f)} = \frac{+e^2}{2p(v_\pi + v_p)\sin^2(\chi/2)} \left[\frac{\mu_p v_\pi v_p}{2c^2} + \text{smaller terms}\right]$$

where v_π and v_p are the pion and proton velocities in the c.m., c = the velocity of light, and μ_p = the magnetic moment of the proton (in nuclear magnetons.)

Phase Shifts from the Maximum-Likelihood Analysis

To investigate the effect of possible systematic error in the measured angular distribution at the small- and large-angle ends, the data were analyzed for both the full angular interval 45° to 135° and the restricted interval 60° to 120°. In addition, to check the effect of including the three possible elastic carbon events (all of which occurred at forward angles), the full angular interval data were analyzed both with and without these events.

Table I

Maximum likelihood phase shift analysis. I: $45^\circ < \chi < 135^\circ$, 38 certain + 3 probable hydrogen events. II: $45^\circ \leq \chi \leq 135^\circ$, 38 certain hydrogen events. III: $60^\circ \leq \chi \leq 120^\circ$, 28 certain + 1 probable hydrogen events. II' is an example of a second (unfavored) solution corresponding to the data of II. (See Fig. 10.) The quoted uncertainties represent the spread of the likelihood function at half-maximum.

Data	a_3	a_{33}	a_{31}
I	$- 0.050 \pm 0.006$	$+ 0.008 \pm 0.009$	$\equiv 0$
II	$- 0.048 \pm 0.006$	$+ 0.011 \pm 0.009$	$+ 0.002 \pm 0.016$
III	$- 0.047 \pm 0.007$	$+ 0.020 \pm 0.013$	$- 0.003 \pm 0.014$
II'	$+ 0.025 \pm 0.010$	$- 0.053 \pm 0.005$	$\equiv 0$

The results for the three selections from the data are summarized in Table I. The likelihood function for case II is mapped in Fig. 10.

Discussion of the Phase-Shift Analysis

The above analysis gives an internally consistent, fairly well defined value for the S-wave scattering phase shift a_3. That the large uncertainty in the value of the P-wave phase shifts does not affect appreciably the determination of a_3 is also apparent from the following results: If a_{33} is assigned the value 0.024 given by the Chew-Low[28] theoretical fit to the higher energy results, and a_{31} is neglected, the maximum-likelihood values of a_3 are - 0.047, - 0.044 (see Fig. 10), and - 0.047 for the data of I, II, and III, respectively.

The more extended analysis, performed for the data of II only, discloses a second set of phase shifts (labeled II'), characterized by positive a_3 and large negative a_{33}. The relative likelihoods favor the accepted set (with negative a_3) by a ratio of approximately 8 to 1 (see Fig. 10). The large value of $|a_{33}|$ required by the reversed sign solution is roughly twice the value obtained by extrapolation from higher energies. The two sets of phase shifts give very different differential cross sections at angles χ beyond the 135° limit of our angular distribution.

The data do not provide a good determination of the P-wave phase shifts. The value determined for a_3 depends largely on the total number of

events found, while the determination of a_{33} depends largely on the relatively few events found at the large- and small-angle ends of the angular distribution. The determination of a_{33} is thus plagued by poor statistics. The ends of the angular distribution, moreover, may be subject to systematic errors in the weight function and in the effect of obtaining spurious events at forward angles by having pions from the steeply-rising Coulomb differential scattering cross section increase their angle by multiple scattering in the target and detector. Although these systematic errors are estimated to be small, the observed depression of the value for a_{33} for cases I and II relative to case III is in the direction of too many forward (and too few backward) events.

The values quoted for a_{31} (for II and III) were obtained by varying this phase shift (to maximize the likelihood function) with a_3 and a_{33} held at the values which had maximized the likelihood under the initial assumption of $a_{31} \equiv 0$. The resulting small values found for a_{31} in each case did not produce an appreciable change in the maximizing value of a_{33}. The likelihood "surface" above the plane of the a_{33}, a_{31}-axes is seen, from the large uncertainties quoted, to be exceedingly flat, so that the location of a maximum is difficult--and not highly significant.

The differential cross sections determined by the sets of phase shifts found for the selections from the data II, II', and III are plotted in Fig. 11, where their fit to the experimental points representing the indicated coarse grouping of the data may be compared.

To summarize: the above analysis gives the following best values for the pion-proton scattering phase shifts at a relative momentum, $\eta \equiv p_{c.m.}/m_\pi c = 0.49$:

$$a_3 = -0.048 \pm 0.07,\ a_{33} = +0.013 \pm 0.013,\ a_{31} = 0.000 \pm 0.016.$$

VI. DISCUSSION

This experiment provides little information with regard to the P-wave scattering, other than a general agreement of the magnitude of a_{33} with the extrapolated value specified by the Chew-Low phenomenological theory[28] ($a_{33} = 0.0238$) and the value given by the Fermi-Orear recipe:[29] $a_{33} = 0.235\,\eta^3 = 0.0280$.

The experiments at 113 and 120 Mev,[7] and the strict stipulation of the causality requirement for the resonance behavior of the scattering,[8] both determine the sign of a_{33} to be positive. Reversed-sign solutions, not favored by the data in any event, can thus certainly be discarded.

The measured value of the S-wave phase shift, a_3, at 25.0 ± 3.5 Mev, appears sufficiently well determined to permit the statement that this experiment confirms the current view that a_3 does not change sign in this energy region.

The momentum dependence of a_3 is still poorly known. The available experimental determinations of a_3[30] are plotted in Fig. 12. The straight-line fit, $a_3 \propto -\eta$, made by Orear[29] is shown, as well as a least-squares fit to the presently available data, including an η^3 dependence. The predicted zero-energy slopes are almost identical: $\frac{a_3}{\eta} = -0.110$ and -0.105, respectively. Values for this quantity can also be inferred from various combinations of data provided by other low-energy experiments. These experiments consist of the work on mesic atoms, (M)[31] giving an average value for $(a_1 + 2a_3)/3\eta$; the very low-energy negative pion direct-scattering cloud chamber results of Lederman, (L)[9] et al. giving $(2a_1 + a_3)/\eta$; and the measurements of the total charge-exchange cross section between 20 and 42 Mev by Spry, (S)[32] giving $(a_1 - a_3)/\eta$. In addition, the Panofsky measurement (P)[33] of the ratio $(\pi^- + p \rightarrow N + \pi^0)/(\pi^- + p \rightarrow N + \gamma)$ combined with photomeson-production results near threshold,[34] and with detailed balance arguments, gives a value for $(a_1 - a_3)/\eta$ at zero energy that is some 30% lower than that inferred from Spry's results. These experiments, taken in the combinations LM, MS, LS, MP, and LP give the values -0.122, -0.109, -0.097, -0.083, -0.047 for $a_{3/\eta}$.[43] Either of the two momentum dependences given above are thus seen to be in agreement with the data pertinent to the zero-energy slope, with the possible exception of the results of the analysis of the Panofsky and photomesic effects.

ACKNOWLEDGMENTS

The encouragement and counsel generously provided by Professor Chaim Richman are gratefully acknowledged.

The authors wish to thank Mr. James Vale, the cyclotron crew, and the members of Professor Richman's group, who all made the exposure possible; Mr. Robert Mathewson for assistance in the design and operation of styrofoam liquid hydrogen targets; Mrs. Edith Goodwin and Miss Irene d'Arche for scanning aid; and Mrs. Bonnie Gronlund for the maximum-likelihood computations.

This work was performed under the auspices of the U. S. Atomic Energy Commission.

REFERENCES

General references for the introduction are:

1. Proceedings of the Fourth Annual Rochester Conference (Jan. 1954),
2. Proceedings of the Fifth Annual Rochester Conference (Jan.-Feb. 1955), and
3. H. A. Bethe and F. de Hoffman, "Mesons and Fields," Row, Peterson, and Co., Vol. II.

---

4. J. Orear, Phys. Rev. 98, 239A (1955).
5. See, for example, H. A. Bethe, Phys. Rev. 90, 994 (1953).
6. J. Orear, J. J. Lord, and A. B. Weaver, Phys. Rev. 93, 575 (1954); D. Bodansky, A. Sachs, and J. Steinberger, Phys. Rev. 93, 1367. (1954); J. P. Perry, and C. E. Angell, Phys. Rev. 91, 1289 (1953).
7. J. Orear, Phys. Rev. 96, 1417 (1954); G. Puppi, Ref. 2, p. 9.
8. R. Karplus and M. Ruderman, Phys. Rev. 98, 771 (1955); H. L. Anderson, W. C. Davidon, and U. E. Kruse, Phys. Rev. (in press).
9. M. C. Rinehart, K. C. Rogers, and L. M. Lederman, Bull. Amer. Phys. Soc. 30, No. 3, 73 (1955); also Nevis Cyclotron Laboratory Report No. 12, June 1955.
10. W. F. Cartwright, C. Richman, M. N. Whitehead, and H. A. Wilcox, Phys. Rev. 91, 677 (1953).
11. C. Richman, M. Skinner, J. Merritt, and B. Youtz, Phys. Rev. 80, 900 (1950).
12. M. Camac, Rev. Sci. Instr. 22, 197 (1951).
13. B. Rankin, Rev. Sci. Instr. 25, 675 (1954).
14. E. D. Courant, M. S. Livingston, and H. S. Snyder, Phys. Rev. 88, 1190 (1952).
15. J. J. Lord, Phys. Rev. 81, 901 (1951).
16. See A. Beiser, Rev. Mod. Phys. 24, 273 (1952).
17. R. W. Birge, L. T. Kerth, C. Richman, D. H. Stork, and S. L. Whetstone, "Techniques for Handling and Processing Emulsion Stacks," University of California Radiation Laboratory Report No. UCRL-2690, Sept. 1954.
18. A. D. Dainton, A. R. Gattiker, and W. O. Lock, Phil. Mag. 42, 396 (1951).
19. W. A. Aron, "The Passage of Charged Particles through Matter," (Thesis), University of California Radiation Laboratory Report No. UCRL-1325, April 1951.

20. H. Fay, K. Gottstein, and K. Hain, Suppl. Nuovo cimento 11, 234 (1954).
21. A. Oliver, Rev. Sci. Instr. 25, 326 (1953); O. Heinz, Phys. Rev. 94, 1728 (1954).
22. R. W. Birge, private communication.
23. H. L. Anderson, E. Fermi, R. Martin, and D. E. Nagle, Phys. Rev. 91, 155 (1953).
24. L. Van Hove, Phys. Rev. 88, 1358 (1952).
25. J. Ashkin, and L. Smith, Tech. Report No. 1, Carnegie Tech. (1953).
26. F. T. Solmitz, Phys. Rev. 94, 1799 (1954).
27. F. T. Solmitz, unpublished notes; C. Wright and J. Orear, private communications; see also J. Orear, J. J. Lord, and A. B. Weaver, Phys. Rev. 93, 575 (1954); J. Orear, Phys. Rev. 96, 1417 (1954).
28. Ref. 2, p. 23.
29. J. Orear, Phys. Rev. 96, 176 (1954); see also J. Orear, Nevis Cyclotron Lab. Report No. 11, May 1955.
30. 24 Mev: J. Orear, private communication and Proceedings of the Fifth Annual Rochester Conference (1955), p. 18.
40 Mev: J. P. Perry and C. E. Angell, Phys. Rev. 91, 1289 (1953).
45 Mev: J. Orear, J. J. Lord, and A. B. Weaver, Phys. Rev. 93, 575 (1954).
61.5 Mev: D. Bodansky, A. Sachs, and J. Steinberg, Phys. Rev. 93, 1367 (1954).
78 Mev: H. L. Anderson, E. Fermi, R. Martin, and D. E. Nagle, Phys. Rev. 91, 155 (1953).
113 Mev: J. Orear, Phys. Rev. 96, 1417 (1954).
120 Mev (a): G. Puppi, Ref. 2, p. 9 (1955).
120 Mev (b): Same as 78-Mev ref.
135 Mev: Same as 78-Mev ref.
165 Mev: H. L. Anderson and M. Glicksman, Phys. Rev. (in press).
189 Mev: H. L. Anderson, W. C. Davidon, M. Glicksman, and U. E. Kruse, Phys. Rev. (in press).
217 Mev: M. Glicksman, Phys. Rev. 94, 1335 (1954).
31. M. Stearns, M. B. Stearns, S. DeBenedetti, and L. Leipuner, Phys. Rev. 97, 240 (1955); 96, 804 (1954); 93, 1123 (1954); see Ref. 2, p. 169 ff.
32. W. J. Spry, Phys. Rev. 95, 1295 (1954).

33. W. K. H. Panofsky, R. L. Aamodt, and J. Hadley, Phys. Rev. 81, 565 (1951).

34. See G. Bernardini and E. L. Goldwasser, Phys. Rev. 95, 857 (1954).

35. Ref. 2, p. 18, Table V.

LEGENDS FOR FIGURES

Fig. 1. Experimental arrangement.

Fig. 2. Scattering target and detector, plan view.

Fig. 3. Scattering target and detector, vertical section.

Fig. 4. Pion beam, integral-range measurements in copper.

Fig. 5. Pion beam, projected range measurements in emulsion. (Arrow from solid circle points to the measured mean projected range; arrow from open circle indicates the mean range corrected for scattering.)

Fig. 6. Pion beam, intensity distributions.

Fig. 7. The kinematic analysis of all otherwise acceptable scattering events found in the interval $35^\circ \leq \chi \leq 135^\circ$. (The dots (·) correspond to the assumption of elastic scattering from carbon, the limits (I) to the assumed scattering from hydrogen at the near and far side of the target.)

Fig. 8. Emulsion-distortion correction curve, from measurements of five steep tracks.

Fig. 9. The weight factor, $F(\chi)$.

Fig. 10. Maximum-likelihood phase-shift analysis.

Fig. 11. The differential scattering cross section.

Curve II: 38 events, $45^\circ \leq \chi \leq 135^\circ$, $a_3 = -0.048$, $a_{33} = +0.011$, $a_{31} = 0$;

Curve II': Reversed sign solution, $a_3 = +0.025$, $a_{33} = -0.052$, $a_{31} = 0$.

Curve III: 29 events, $60^\circ \leq \chi \leq 120^\circ$, $a_3 = -0.047$, $a_{33} = +0.020$, $a_{31} = 0$.

Fig. 12. Momentum dependence of the S-wave phase shift, a_3. (See Reference 30.)

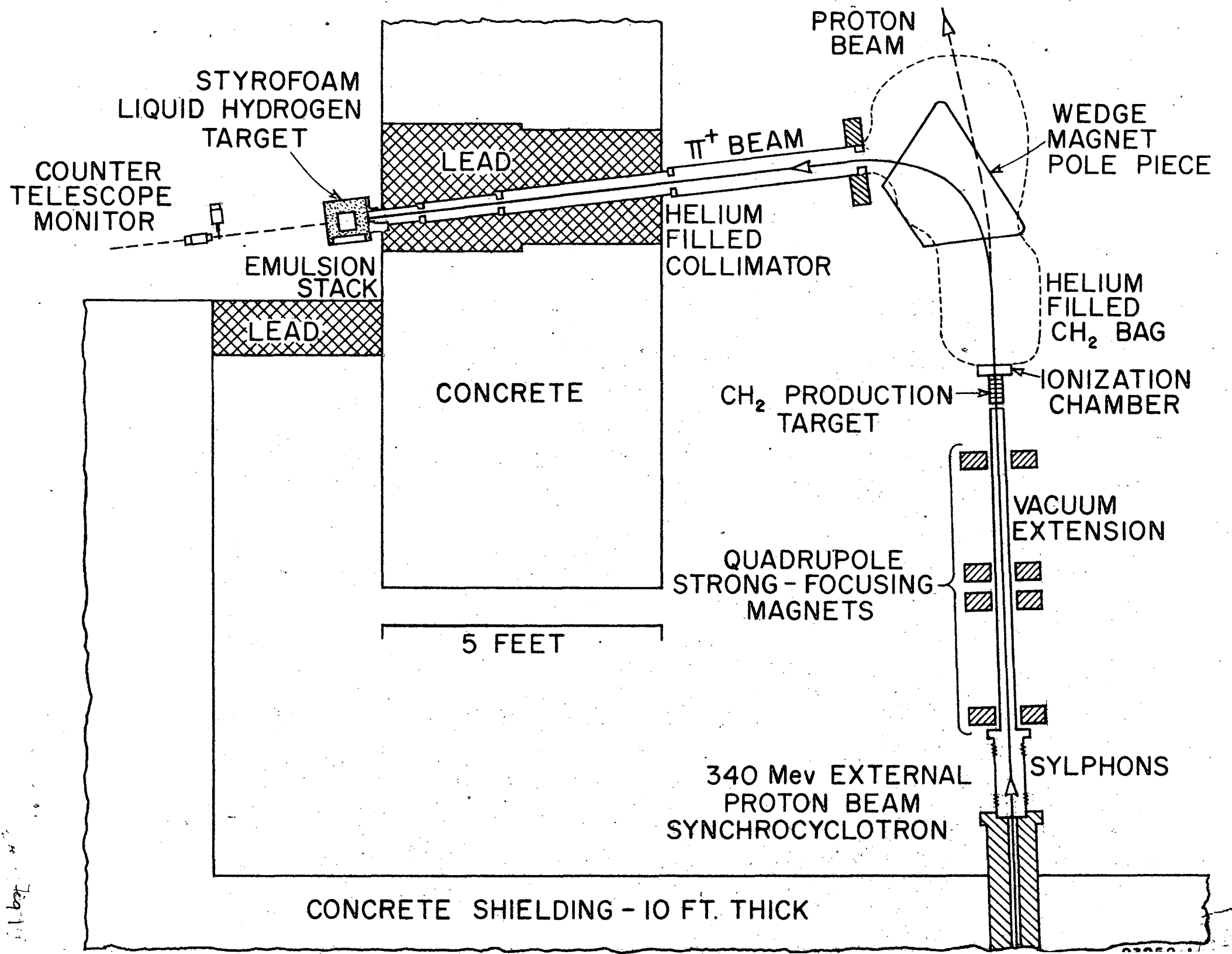
PROTON BEAM
STYROFOAM LIQUID HYDROGEN TARGET
LEAD
π^+ BEAM
WEDGE MAGNET POLE PIECE
COUNTER TELESCOPE MONITOR
HELIUM FILLED COLLIMATOR
EMULSION STACK
LEAD
HELIUM FILLED CH_2 BAG
CONCRETE
CH_2 PRODUCTION TARGET
IONIZATION CHAMBER
VACUUM EXTENSION
QUADRUPOLE STRONG-FOCUSING MAGNETS
5 FEET
SYLPHONS
340 Mev EXTERNAL PROTON BEAM SYNCHROCYCLOTRON
CONCRETE SHIELDING - 10 FT. THICK

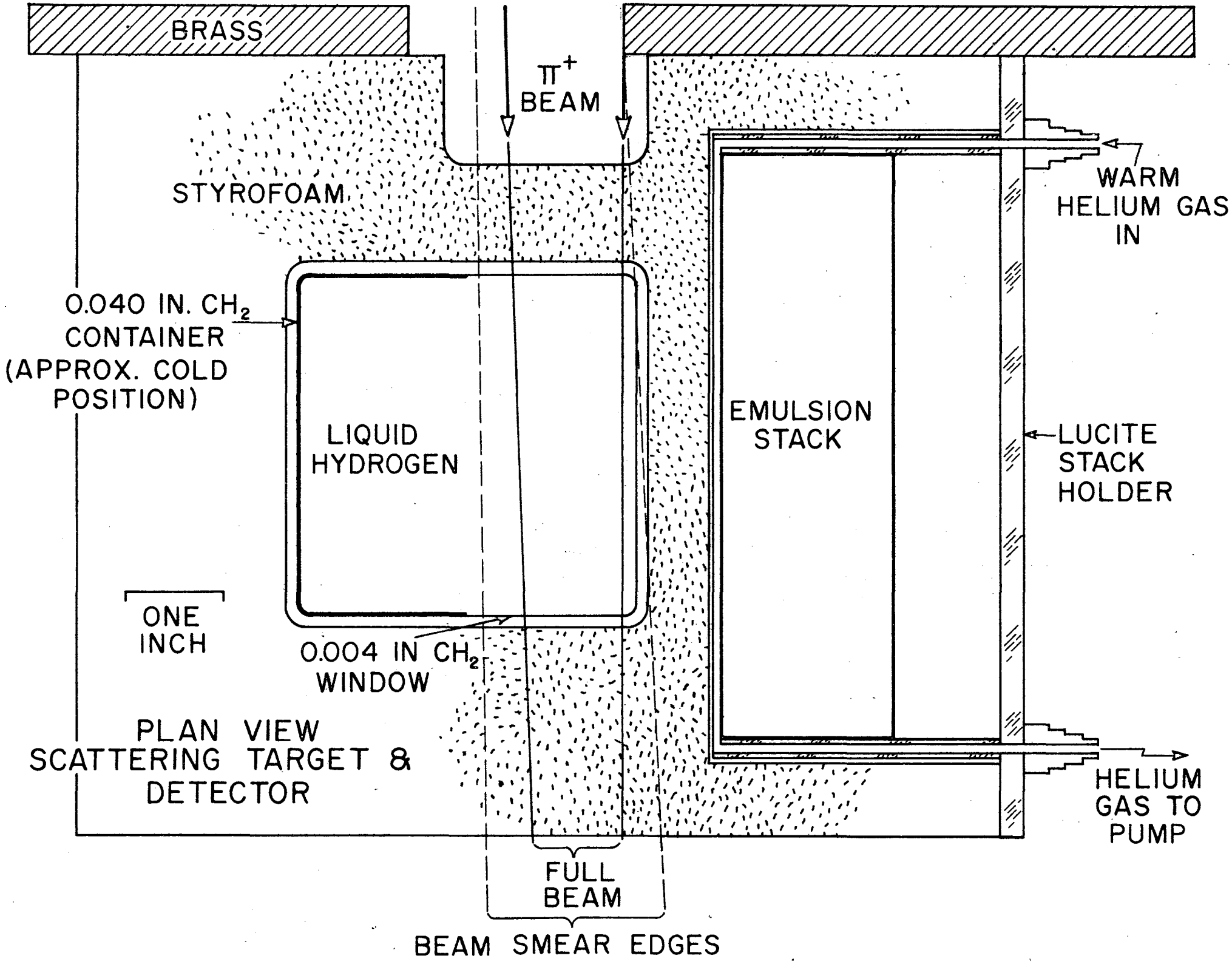
BRASS
π^+ BEAM
STYROFOAM
WARM HELIUM GAS IN
0.040 IN. CH_2 CONTAINER (APPROX. COLD POSITION)
LIQUID HYDROGEN
EMULSION STACK
LUCITE STACK HOLDER
ONE INCH
0.004 IN CH_2 WINDOW
PLAN VIEW SCATTERING TARGET & DETECTOR
HELIUM GAS TO PUMP
FULL BEAM
BEAM SMEAR EDGES
23251-1

fig. 2

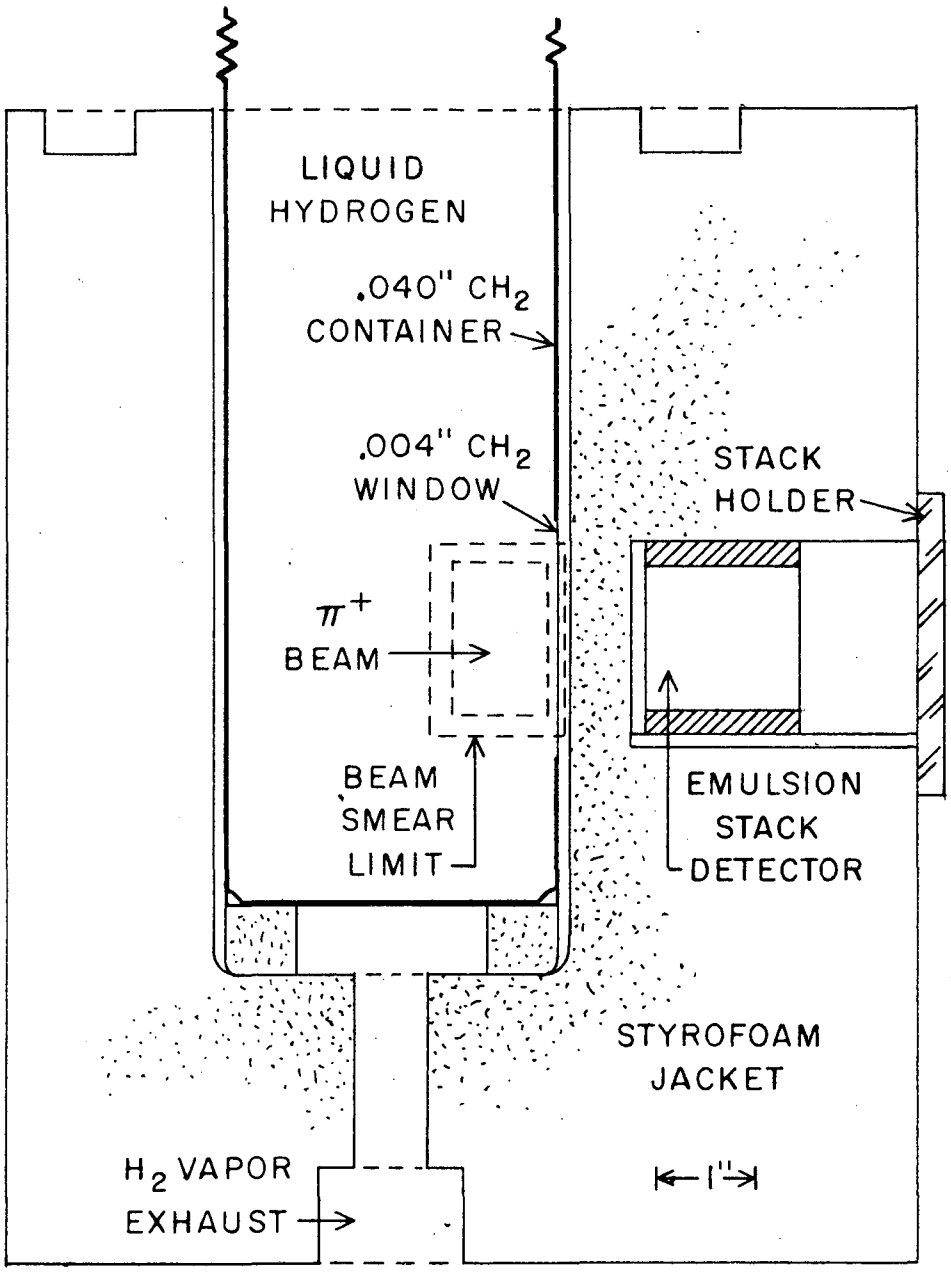
LIQUID
HYDROGEN
.040" CH_2
CONTAINER
.004" CH_2
WINDOW
STACK
HOLDER
π^+
BEAM
BEAM
SMEAR
LIMIT
EMULSION
STACK
DETECTOR
STYROFOAM
JACKET
H_2 VAPOR
EXHAUST
1"

Fig. 3

24026-1

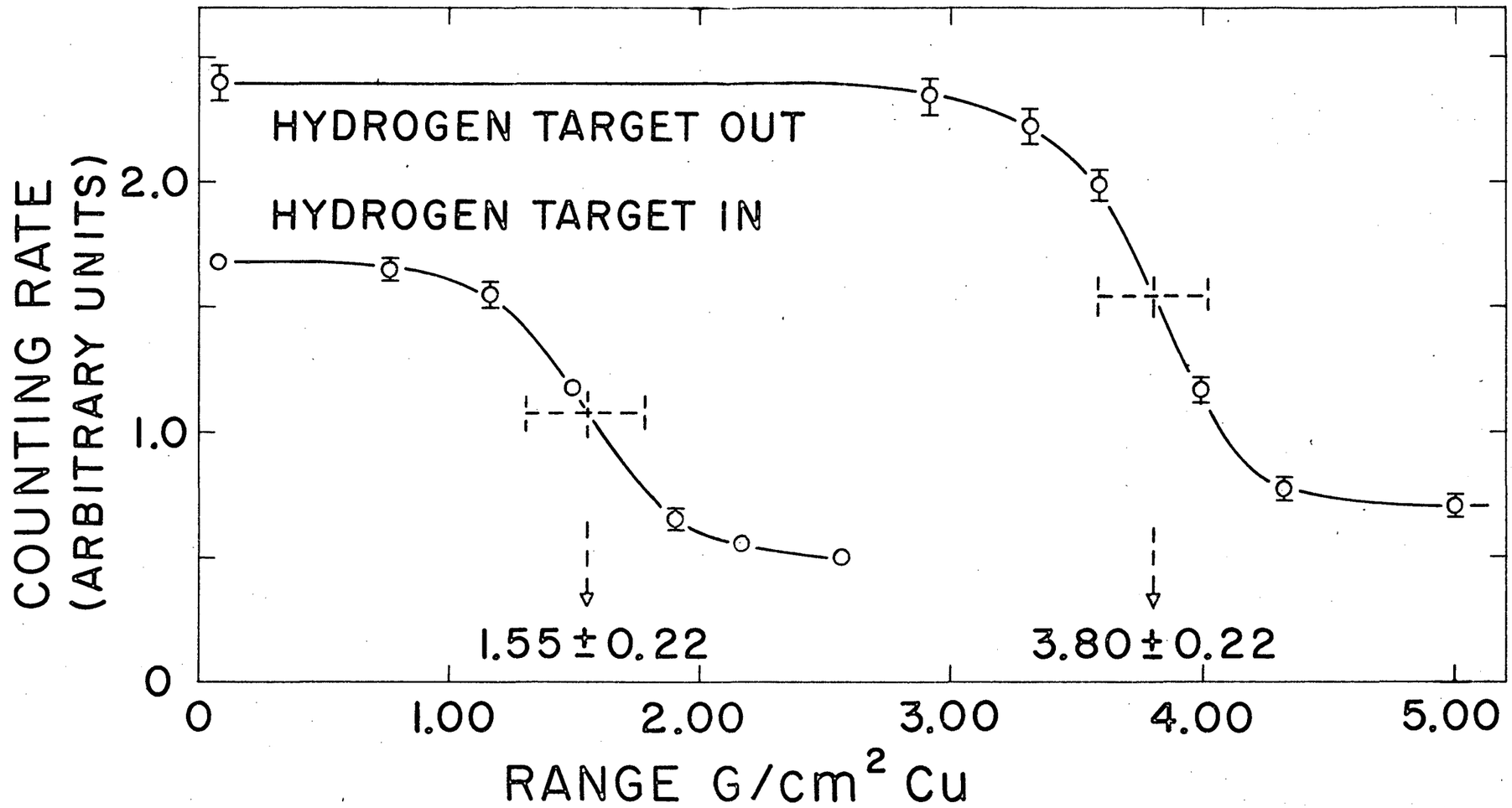
HYDROGEN TARGET OUT
HYDROGEN TARGET IN
COUNTING RATE
(ARBITRARY UNITS)
2.0
1.0
0
1.55 ± 0.22
3.80 ± 0.22
0
1.00
2.00
3.00
4.00
5.00
RANGE G/cm² Cu

Fig. 4

24027 - 2

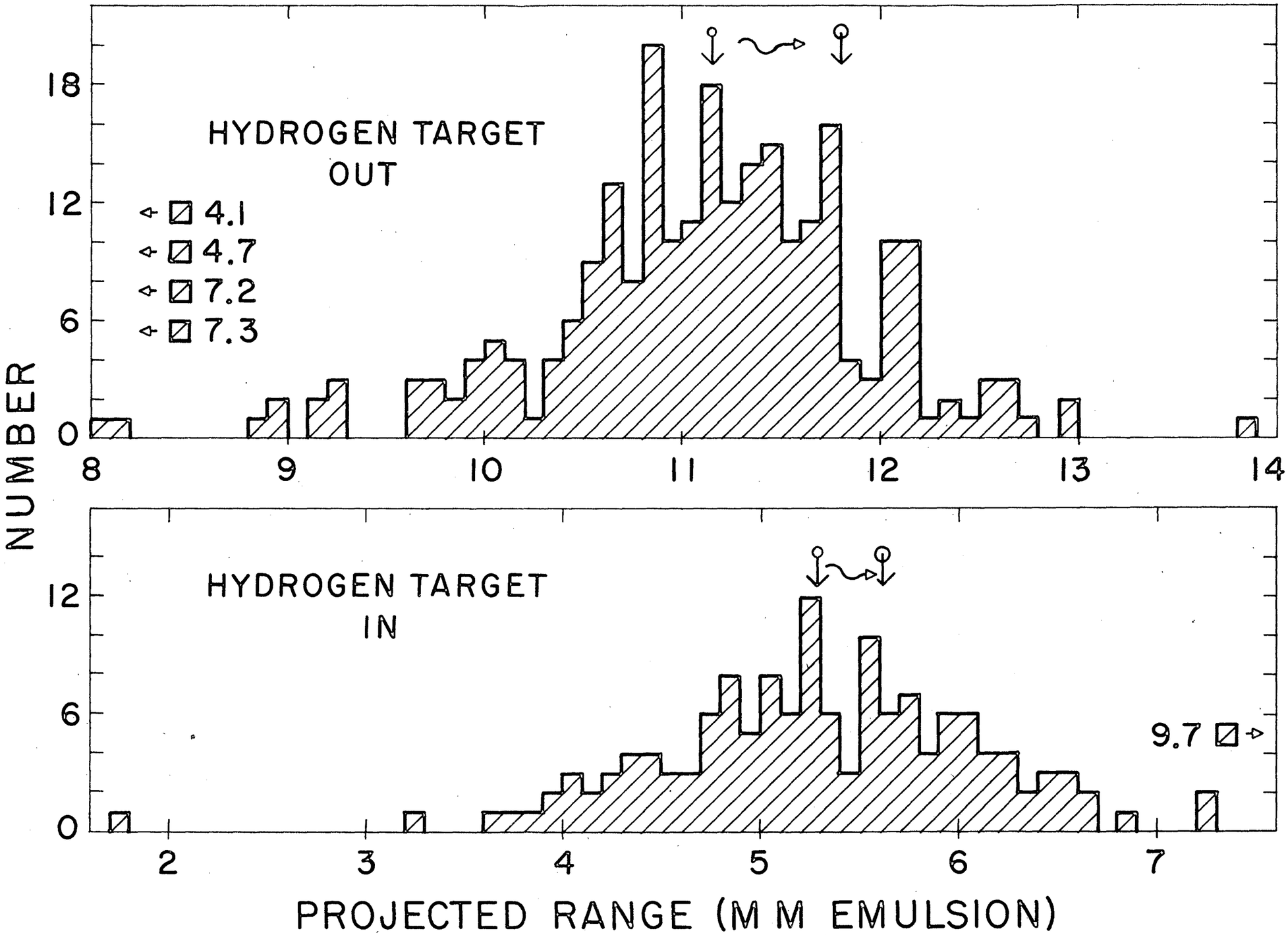
HYDROGEN TARGET
OUT
4.1
4.7
7.2
7.3
NUMBER
0
6
12
18
8
9
10
11
12
13
14
HYDROGEN TARGET
IN
9.7
0
6
12
2
3
4
5
6
7
PROJECTED RANGE (M M EMULSION)

Fig. 5

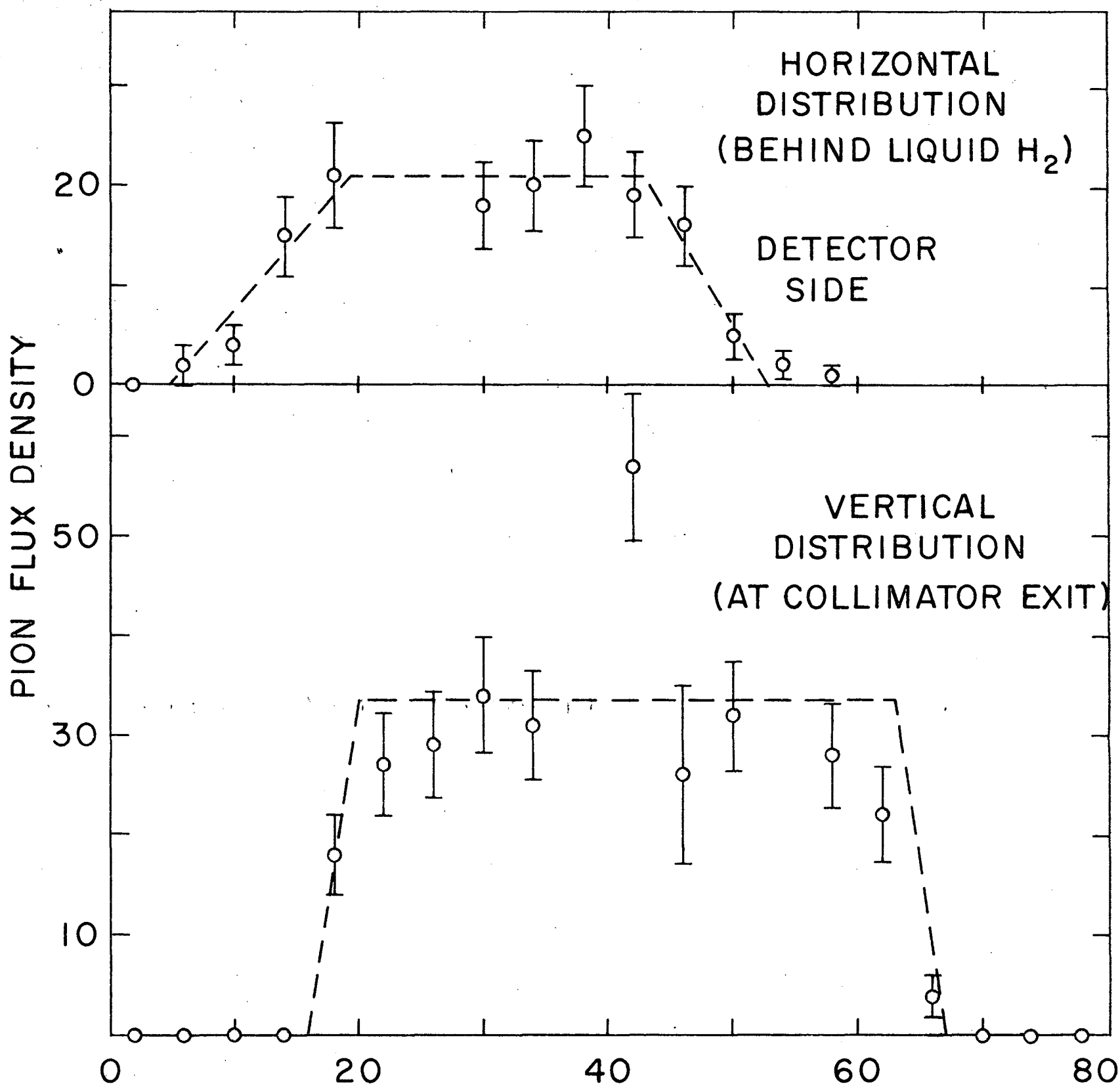
HORIZONTAL
DISTRIBUTION
(BEHIND LIQUID H_2)
DETECTOR
SIDE
VERTICAL
DISTRIBUTION
(AT COLLIMATOR EXIT)
PION FLUX DENSITY
20
0
50
30
10
0
20
40
60
80
DISTANCE (MM)

Fig. 6

24029-2

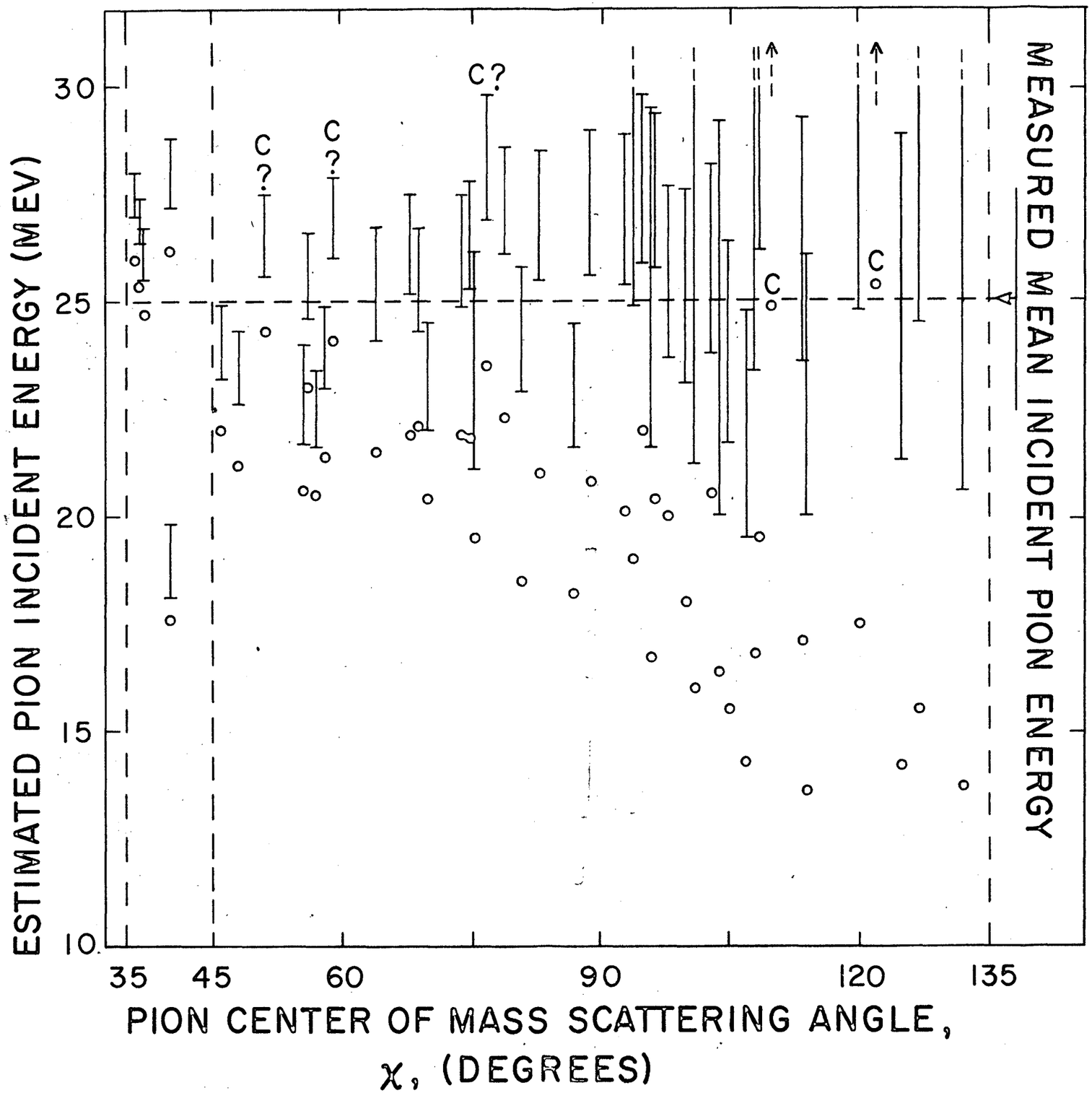
MEASURED MEAN INCIDENT PION ENERGY
ESTIMATED PION INCIDENT ENERGY (MEV)
30
25
20
15
10
C?
C?
C?
C
C
C
35
45
60
90
120
135
PION CENTER OF MASS SCATTERING ANGLE,
χ, (DEGREES)

Fig. 7
24030-2

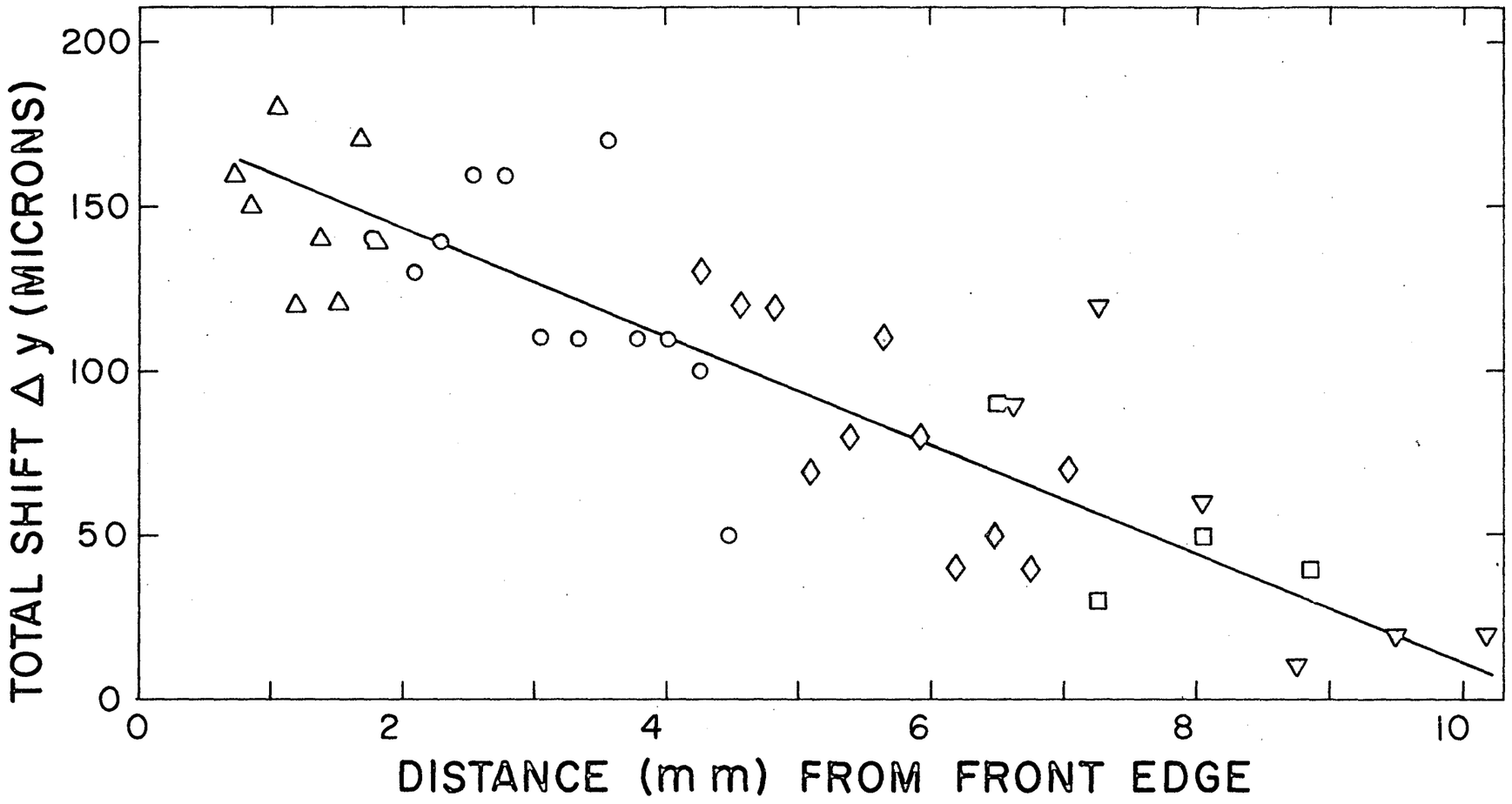
TOTAL SHIFT Δ y (MICRONS)
200
150
100
50
0
0
2
4
6
8
10
DISTANCE (m m) FROM FRONT EDGE

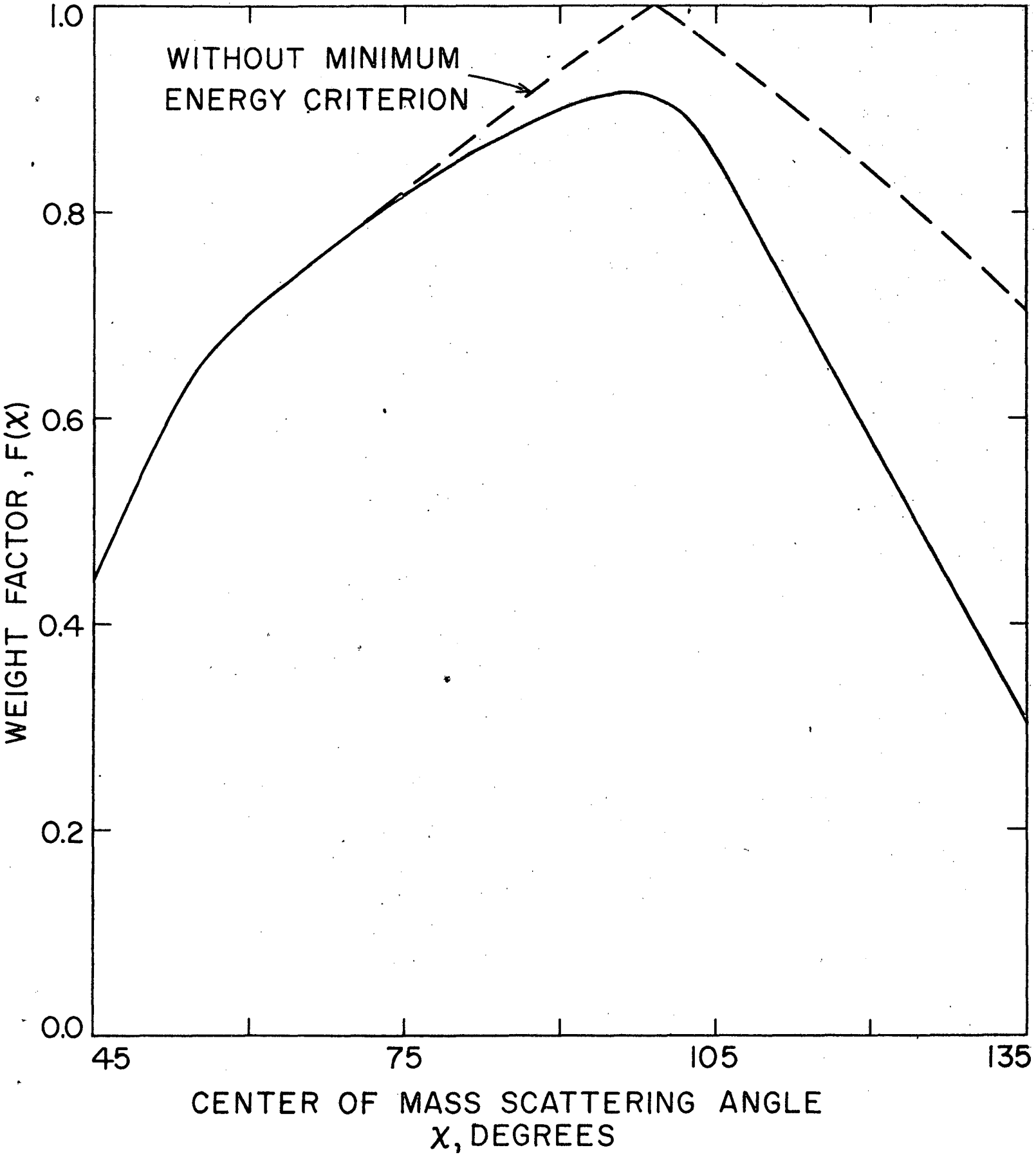
WITHOUT MINIMUM
ENERGY CRITERION
1.0
0.8
0.6
0.4
0.2
0.0
WEIGHT FACTOR, F(χ)
45
75
105
135
CENTER OF MASS SCATTERING ANGLE
χ, DEGREES

Fig 9

24034-1

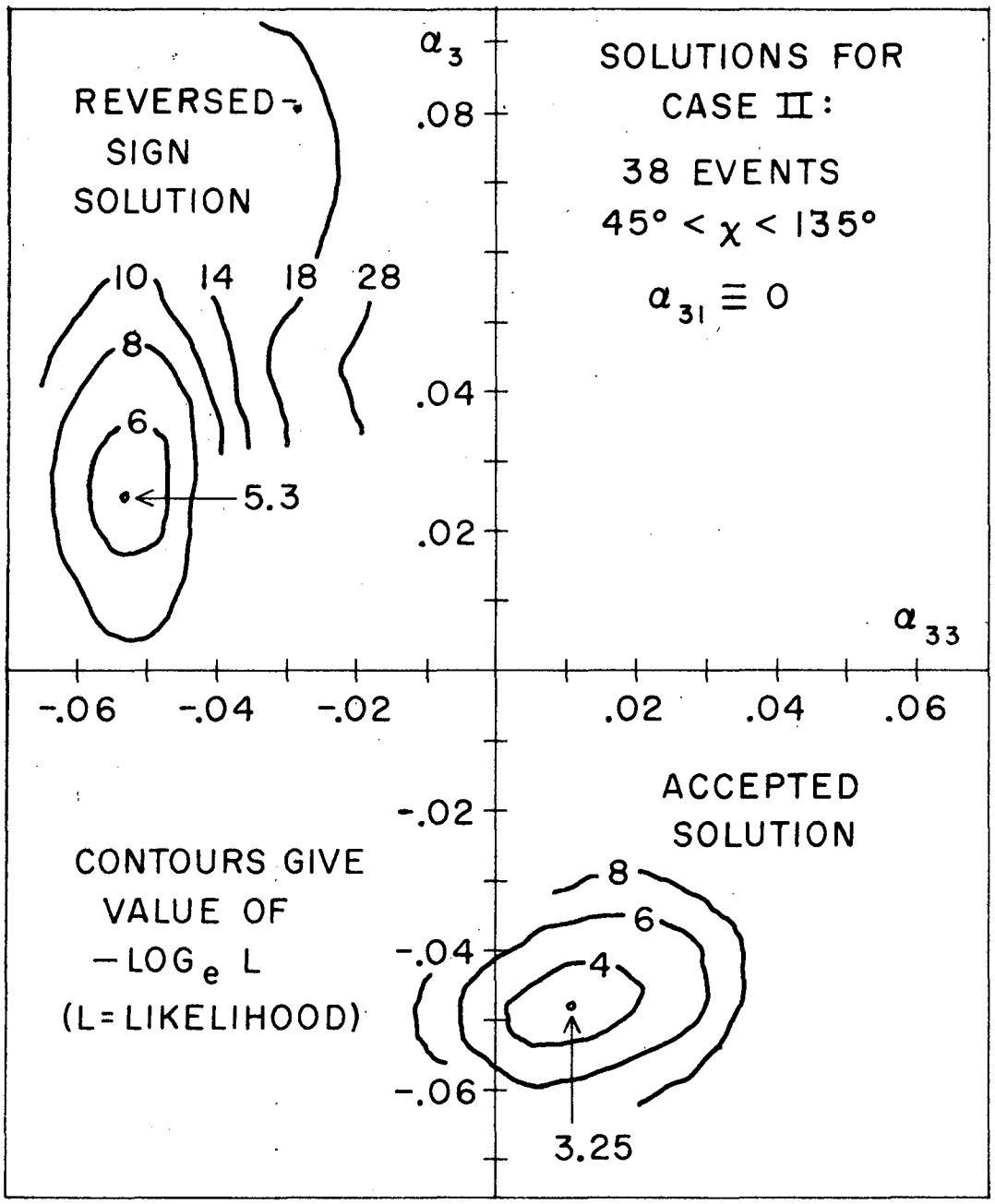

Fig. 10

24036-1

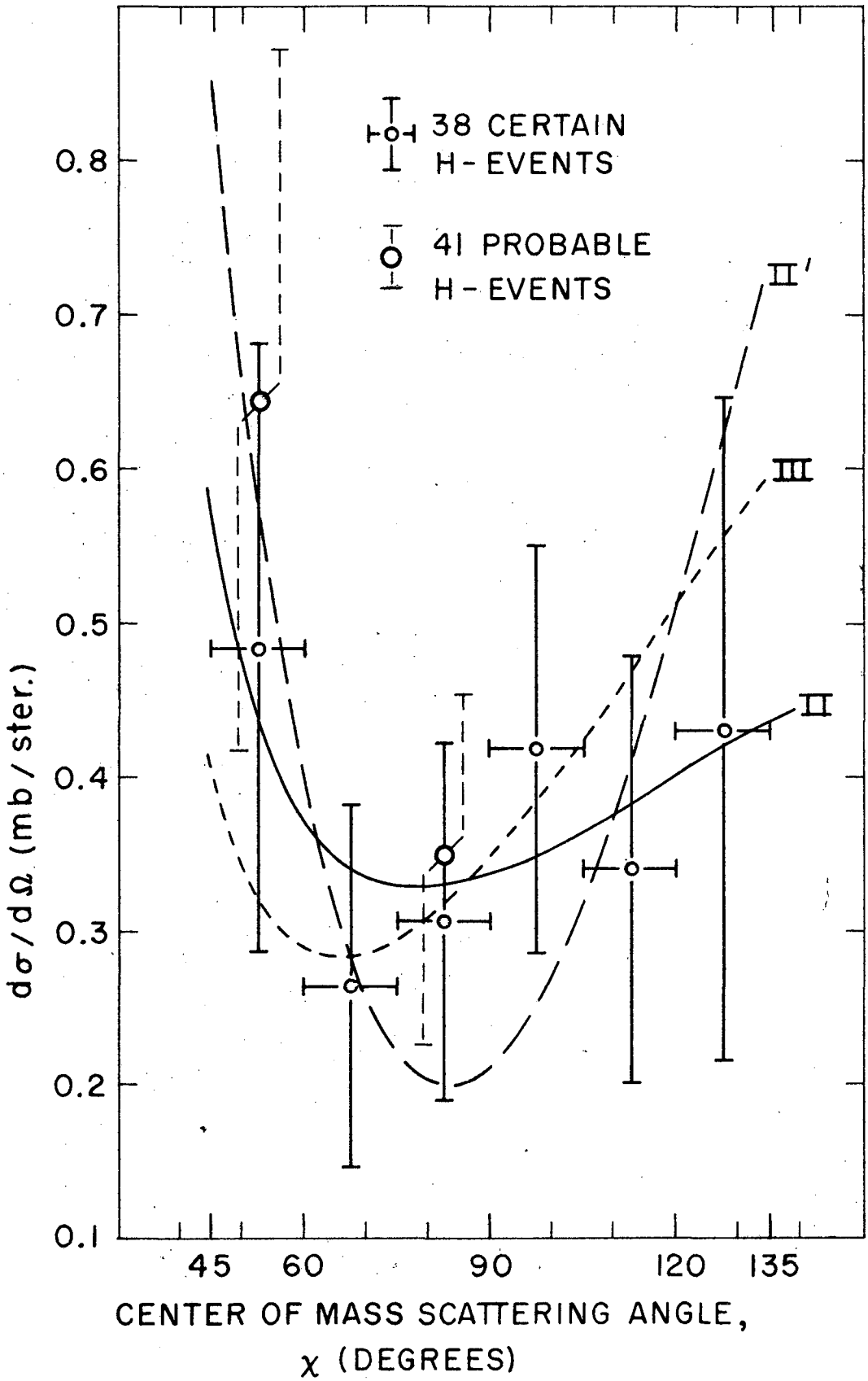

Fig. 11

24035-1

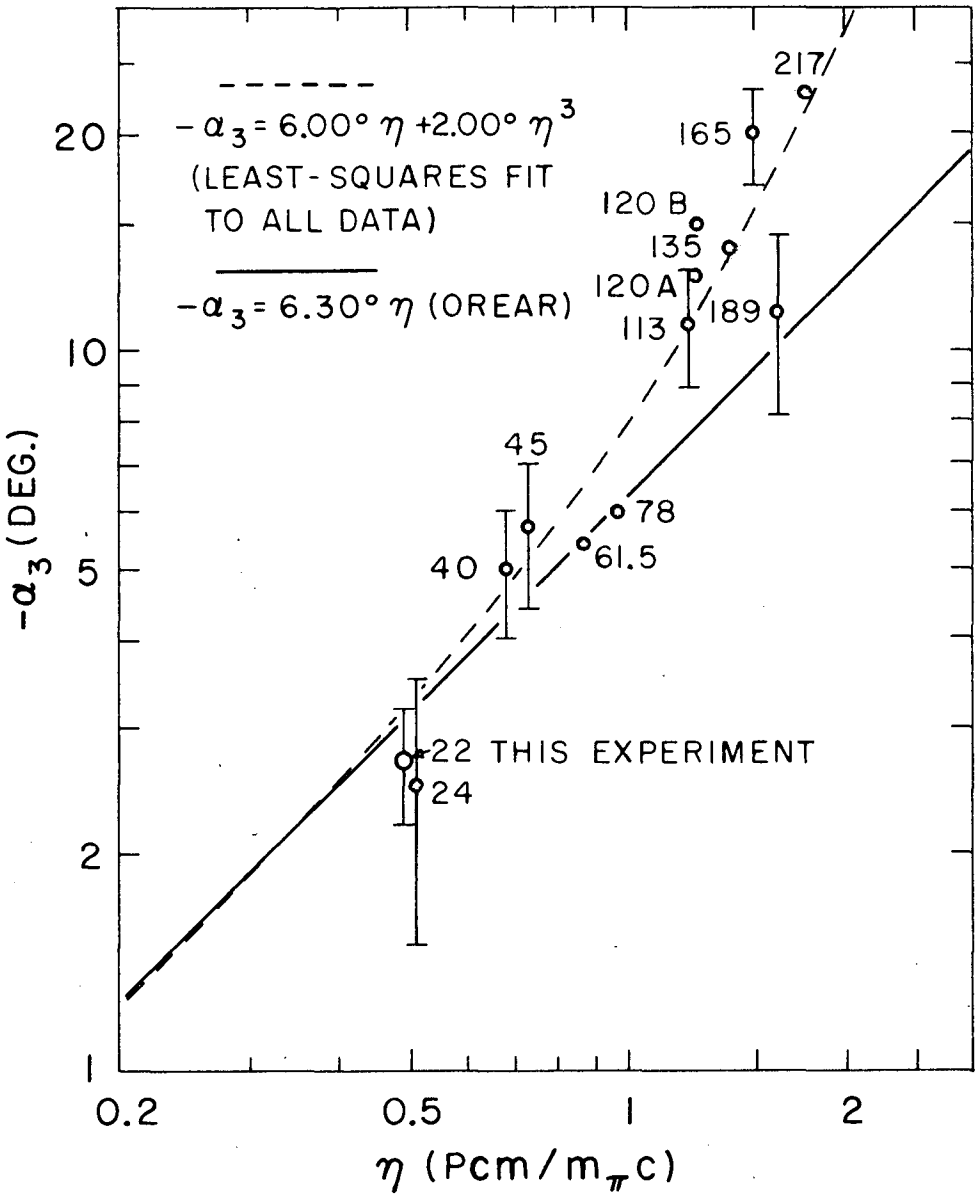

Fig. 12

24037-1